

Nonlinear Proportional-Integral-Derivative Control of a Multi-input Multi-output Distillation Column Process Incorporating Genetic Algorithms

Tewodros Asfaw GEBRETSADIK¹, Gang-Gyoo JIN², Jaesung KWON³, Jongkap AHN^{4*}

¹ Department of Electrical Power and Control Engineering, Adama Science and Technology University, Kebele 14, Adama, P.O. Box 1888, Ethiopia
tewodros.asfaw@astu.edu.et

² School of Electrical Engineering and Computing, Adama Science and Technology University, Kebele 14, Adama, P.O. Box 1888, Ethiopia
gj30@astu.edu.et

³ Department of Mechanical Systems Engineering, Gyeongsang National University, 2, Tongyeonghaean-ro, Tongyeong-si, 53064, Republic of Korea
jkwon@gnu.ac.kr

⁴ Training Ship Operation Center, Gyeongsang National University, 2, Tongyeonghaean-ro, Tongyeong-si, 53064, Republic of Korea
jongkap.ahn@gnu.ac.kr (*Corresponding author)

Abstract: Distillation columns are integral components of chemical processing plants. Their inherent multi-input multi-output (MIMO) configuration, characterized by interdependent inputs and outputs, poses significant challenges for controller design. This paper presents a comprehensive comparative analysis of various control strategies for managing the top and bottom composition for a distillation column, with a focus on the impact of decoupling. Employing the Wood-Berry distillation model in order to facilitate the separation of methanol from water, this study examines the effects of feed flow rate disturbances. With the purpose of mitigating or eliminating the cross-interactions between inputs and outputs, a decoupler was designed in order to transform the analysed system into two independent single-input single-output (SISO) systems. Subsequently, nonlinear proportional-integral-derivative (PID) controllers were developed for controlling the distillation column, their parameters being optimized through a genetic algorithm. The obtained simulation results demonstrate that the proposed control system significantly reduces the total error in comparison with the employed conventional PID control system, particularly in terms of setpoint tracking and disturbance rejection.

Keywords: Distillation column, MIMO, Decoupling, Nonlinear PID controller, Genetic algorithm.

1. Introduction

Distillation columns are widely used in chemical and petroleum processing, serving as a crucial unit operation for separating liquid mixtures into their components. This separation process is fundamental in various industries, facilitating the purification and isolation of components from mixtures containing two or more substances (Fard et al., 2016).

Vertical cylindrical columns offer a compact and space-efficient design, enabling numerous stages of vaporisation and condensation within a limited footprint. However, controlling the distillation column processes poses significant challenges. These challenges stem from the system's inherent nonlinearities, its complex multi-input multi-output (MIMO) structure and the unavoidable presence of operational disturbances. Furthermore, the inherent uncertainties within the chemical process complicate modelling and control efforts (Bhattacharjee & Medhi, 2012).

Distillation columns are energy-intensive, consuming roughly one-third of the total energy used in chemical plants. Moreover, various studies

indicate that 40-50% of the energy consumed by the petroleum and chemical industries is dedicated to distillation processes (Tan & Cong, 2023). Enhancing the efficiency of these processes is crucial for conserving energy and reducing emissions in the chemical industry (Tan & Cong, 2023; Carrasco et al., 2021). However, achieving this requires effective modelling and control methods.

To mitigate control interactions, decoupling strategies are implemented (Haji Haji & Monje, 2019). Achieving an optimal system performance requires the precise tuning of controller gains. In this study, a genetic algorithm (GA) is employed to identify the optimal gain set for these controllers. The optimization process is guided by objective functions such as the Integral Absolute Error with Control Signal (IAEU) and the Integral Time-weighted Absolute Error with Control Signal (ITAEU), which are employed to select the most effective controller gains. The performance of the controllers within the proposed system is evaluated based on their steady-state and transient-state responses, with a particular

emphasis on their capabilities in setpoint tracking and disturbance rejection.

Numerous research papers have explored distillation column control systems, employing diverse tuning and optimisation algorithms. As distillation columns are inherently MIMO systems with interconnected parameters, their control is often affected by sluggish responses due to parameter interactions. Decoupling techniques are essential for mitigating these interactions and improving the controller performance.

In (Das et al., 2023), the authors proposed a novel two-degree-of-freedom PID controller structure designed explicitly for processes with integration characteristics, ensuring an effective control performance for both the step- and ramp-type input signals.

Govinda & Arunshankar (2022) studied the control of two-input and two-output systems utilising a sliding mode controller. The controller's parameters are optimised using the Nelder–Mead algorithm to minimise the integral time absolute error criterion.

Nourelhouda & Abdelmadjid (2022) propose a fractional-order PID controller for distillation columns, tuned by using the most significant log modulus method in conjunction with a multi-objective particle swarm optimisation algorithm, aiming to achieve an optimal control performance.

In (Ye et al., 2023), which presents an intelligent optimisation approach for distillation columns, surrogate models were developed using a combination of GA and backpropagation neural networks to enhance design efficiency.

This paper provides a general review of the performance of controllers designed by using a range of optimisation strategies. While the existing control methods demonstrate a satisfactory performance across various environments, they are often affected by process dependencies and an increased number of tuning parameters in comparison with the conventional PID controllers. In this sense, this paper introduces a novel nonlinear PID controller that incorporates a nonlinear gain element in combination with the integral action of a standard PID structure. To optimise the tracking performance for step setpoint changes, the controller parameters are determined based on a process model and a genetic algorithm, while minimising two performance indices. The effectiveness of the proposed controller is validated through simulations of two representative

processes, its performance being compared with that of a conventional linear PID controller.

This paper is organized as follows. Section 2 provides an overview of the modelling of a distillation column with a decoupler. Section 3 describes the enhanced nonlinear PID controller, while Section 4 presents the simulation results and discusses them. Finally, Section 5 includes the conclusion of this paper and refers to possible future research directions.

2. Modelling of a Distillation Column

2.1 Distillation Column and Model

Distillation columns are essentially tall towers. Inside, trays are evenly spaced along the column's height. Each tray incorporates a bubble cap, a crucial component for facilitating mass transfer between the rising vapour and descending liquid. The feed, a mixture of chemicals (specifically two components in the case of fractional distillation), is introduced into the column. The separation process relies on exploiting the differing temperature profiles within the tower to achieve the desired separation of the components.

A distillation column has at least four feedback control loops to govern the distillate concentration, bottom concentration, reboiler level, and reflux rate (Acharya et al., 2016). The control challenge is classified as a MIMO system. This study presents a controller designed to manage distillate and bottom concentrations. A common approach to MIMO control involves the implementation of two separate controllers, each targeting a specific output. Figure 1 illustrates the detailed process related to the distillation column.

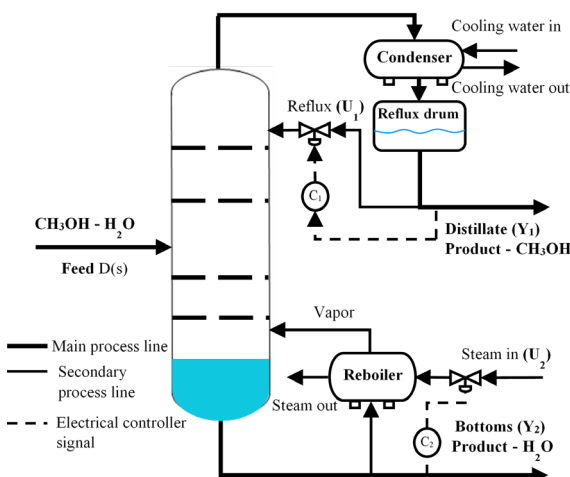


Figure 1. Schematic diagram of the conventional two-point distillation column process (Li et al., 2015)

A simplified mathematical model proposed by Wood and Berry (1973) can be expressed as:

$$\mathbf{Y}(s) = \mathbf{G}_p(s)\mathbf{U}(s) + \mathbf{G}_d(s)D(s), \quad (1a)$$

where $\mathbf{Y} = [Y_1 \ Y_2]^T$ is the output vector, $\mathbf{U} = [U_1 \ U_2]^T$ is the control input vector, and D is the disturbance of the unmeasured flow rate (lb/min). Y_1 and Y_2 are distilled methanol (mol%) and water (mol%), respectively, and U_1 and U_2 represent the reflux flow rate (lb/min) and steam flow rate (lb/min), respectively. The system and disturbance transfer function matrices are given by:

$$\mathbf{G}_p(s) = \begin{bmatrix} G_{11}(s) & G_{12}(s) \\ G_{21}(s) & G_{22}(s) \end{bmatrix}, \quad (1b)$$

$$G_{p11}(s) = \frac{12.8e^{-s}}{16.7s+1}, \quad G_{p12}(s) = -\frac{18.9e^{-3s}}{21s+1}, \quad (1c)$$

$$G_{p21}(s) = \frac{6.6e^{-7s}}{10.9s+1}, \quad G_{p22}(s) = -\frac{19.4e^{-3s}}{14.4s+1}$$

$$\mathbf{G}_d(s) = \begin{bmatrix} G_{d1}(s) \\ G_{d2}(s) \end{bmatrix}, \quad (1d)$$

$$G_{d1}(s) = \frac{3.8e^{-8s}}{14.9s+1}, \quad G_{d2}(s) = \frac{4.9e^{-3s}}{13.2s+1}. \quad (1e)$$

2.2 Design of a Decoupler

For a MIMO system, the system's gain matrix includes columns representing input variables and rows representing output variables. This arrangement allows for the analysis of relative gains in the context of input-output pairs, enabling the identification of the optimal pairings that prioritize the desired interactions and mitigate unwanted cross-coupling. The relative gain array (RGA) analysis is used to determine the best input-output pairings for multivariable process control systems (Pawar & Jadhav, 2018). The RGA can be computed directly from the square gain matrix \mathbf{K} as:

$$RGA = \mathbf{K} \otimes (\mathbf{K}^{-1})^T, \quad (2)$$

where \otimes is the element-wise multiplication of the two matrices. From equations 1(a-e), without considering the disturbances, \mathbf{K} is calculated as:

$$\mathbf{K} = \begin{bmatrix} k_{11} & k_{12} \\ k_{21} & k_{22} \end{bmatrix}, \quad (3a)$$

where

$$k_{11} = \left. \frac{\partial y_1}{\partial u_1} \right|_{u_2=0} = 12.8, \quad (3b)$$

$$k_{12} = \left. \frac{\partial y_2}{\partial u_1} \right|_{u_2=0} = -18.9, \quad (3c)$$

$$k_{21} = \left. \frac{\partial y_1}{\partial u_2} \right|_{u_1=0} = 6.6, \quad (3d)$$

$$k_{22} = \left. \frac{\partial y_2}{\partial u_2} \right|_{u_1=0} = -19.4. \quad (3e)$$

Applying the results of equations 3(a-e) to equation (2), the RGA is obtained as follows:

$$RGA = \begin{bmatrix} 2.0094 & -1.0094 \\ -1.0094 & 2.0094 \end{bmatrix} \quad (4)$$

In accordance with the pairing selection rule outlined in (Nevetha & Suresh, 2016), the (u_1, y_1) and (u_2, y_2) pairings characterised by positive elements are selected, while discarding the (u_1, y_2) and (u_2, y_1) pairings containing negative elements. The following decoupling matrix with a simple structure is considered:

$$\mathbf{M}(s) = \begin{bmatrix} M_{11}(s) & M_{12}(s) \\ M_{21}(s) & M_{22}(s) \end{bmatrix} \quad (5)$$

The block diagram of the distillation column (DC) process with the decoupler is shown in Figure 2.

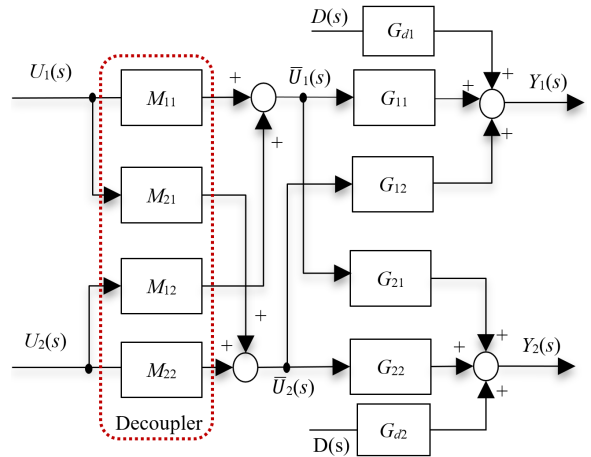


Figure 2. DC process with a decoupler

To exclude the (u_1, y_2) and (u_2, y_1) pairings with the choice $M_{11}=M_{22}=1$ in Figure 2, the following is obtained:

$$M_{12}G_{p11}U_{22} + G_{p12}U_{22} = 0 \quad (6)$$

$$M_{21}G_{p22}U_{11} + G_{p21}U_{11} = 0$$

Then, M_{12} and M_{21} can be calculated from equation (6):

$$M_{12} = -\frac{G_{p12}}{G_{p11}} = \frac{24.66s + 1.48}{21s + 1} e^{-2s} \quad (7)$$

$$M_{21} = -\frac{G_{p21}}{G_{p22}} = \frac{4.89s + 0.34}{10.9s + 1} e^{-4s}$$

Finally, the input–output relationship between the DC process and the decoupler yields:

$$Y(s) = \mathbf{G}_p(s)\mathbf{M}(s)\mathbf{U}(s) + \mathbf{G}_d(s)D(s) \quad (8)$$

To examine the system's characteristics in the frequency domain, Bode diagrams were drawn, which are shown in Figures 3 and 4.

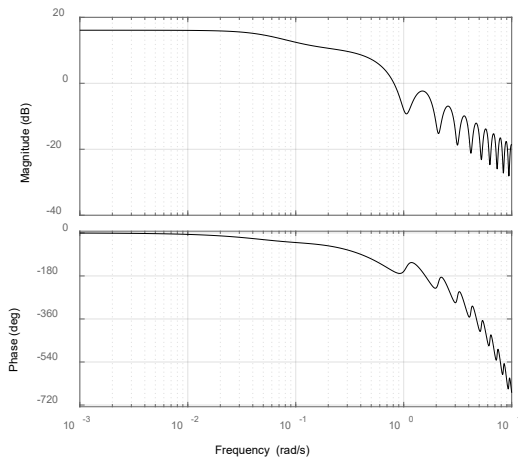


Figure 3. Bode diagram of the open-loop system with the decoupler (from u_1 to y_1)

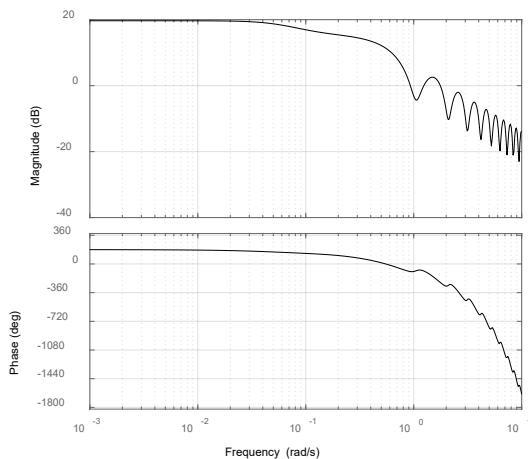


Figure 4. Bode diagram of the open-loop system with the decoupler (from u_2 to y_2)

The transfer function from input u_1 to output y_1 exhibits a gain margin (GM) of 1.36dB, a phase margin (PM) of 19.25° and a bandwidth (BW) of 0.08rad/s, while the transfer function from input u_2 to output y_2 features a GM of 0.77dB, a PM of -51.16° and a BW of 0.1rad/s.

2.3 Steady-state Analysis of the DC With the Decoupler

By applying the final value theorem to equation (8) in the absence of disturbances, the steady-state input-output relationship is derived, yielding the following result:

$$\mathbf{y}_0 = \lim_{s \rightarrow 0} s \left[\mathbf{G}_p(s)\mathbf{M}(s) \frac{\mathbf{u}_0}{s} \right], \quad (9)$$

$$= \begin{bmatrix} 6.3740 & 0.0440 \\ 0.0440 & -9.6320 \end{bmatrix} \mathbf{u}_0$$

where $\mathbf{y}_0 = [y_{10} \ y_{20}]^T$ and $\mathbf{u}_0 = [u_{10} \ u_{20}]^T$. From equation (9), \mathbf{u}_0 can be rendered as:

$$\mathbf{u}_0 = \begin{bmatrix} 1.569 & 0 \\ 0 & -0.1038 \end{bmatrix} \mathbf{y}_0 \quad (10)$$

As expected, using the decoupler shows that u_{10} affects only y_{10} , and similarly u_{20} affects only y_{20} .

3. Design of a Nonlinear PID Controller

The fixed-parameter PID controller, as discussed in subsection 4.1, exhibits satisfactory response characteristics within a nominal operating range. However, its performance can be adversely affected, potentially leading to instability when operating beyond this range. To address the limitations of the traditional PID controller, various nonlinear PID (NPID) controllers have been proposed (Jin & Son, 2019).

3.1 The Existing Nonlinear PID Controller

Linear PID controllers excel when operating within their designed operating range. However, their performance can deteriorate significantly when process dynamics deviates from the expected range, like in the case of unexpected changes. NPID controllers provide advantages for nonlinear processes, such as a smoother operation and an improved resilience to unforeseen disturbances. NPID controllers are harder to design and implement than linear PID controllers due to their increased number of tuning parameters (Jin & Son, 2019; Son & Jin, 2019). This work proposed a novel NPID controller for addressing this problem, enhancing the conventional PID framework. This NPID controller requires only three tuning parameters (Hamdy & Ramadan,

2017). To mitigate the limitations of traditional PID controllers, specifically the integral action's susceptibility to overshoot, oscillations, and integral windup under dynamic conditions, the NPID controller incorporates a nonlinear gain. This nonlinear gain dynamically adjusts the error signal fed to the integrator, improving the controller performance during sudden setpoint changes and disturbances. The time-domain representation of this controller is given by:

$$\begin{aligned} u(t) &= u_p(t) + u_i(t) + u_d(t) \\ u_p(t) &= K_p e(t) \\ u_i(t) &= K_i \int v(t) dt \\ \frac{T_d}{N} \frac{du_d(t)}{dt} + u_d(t) &= -K_d \frac{de(t)}{dt} \end{aligned} \quad (11)$$

where u_p , u_i , and u_d are the proportional, integral, and derivative actions, respectively. K_p , K_i , and K_d are the proportional gain, integral gain, and derivative gain, respectively. T_d is given by $\frac{K_d}{K_p}$. Meanwhile, $v(t)$ is the scaled error expressed as:

$$v(t) = k(e)e(t), \quad (12)$$

where $k(e)$ is a function of e represented by:

$$k(e) = \exp\left[-\frac{e^2(t)}{2\sigma^2}\right], \quad (13)$$

where $\sigma (\neq 0)$ denotes the biggest change in the setpoint value between steps. Noise sensitivity is a key limitation of the ideal derivative action. A low-pass filter is thus used to mitigate the risk of instability from high-frequency noise amplification. N , a user-defined parameter, is selected based on the noise environment, its typical values ranging from 5 to 20. For this study, N was chosen to be 10 (O'Dwyer, 2009). Figure 5 depicts the structure of the NPID controller.

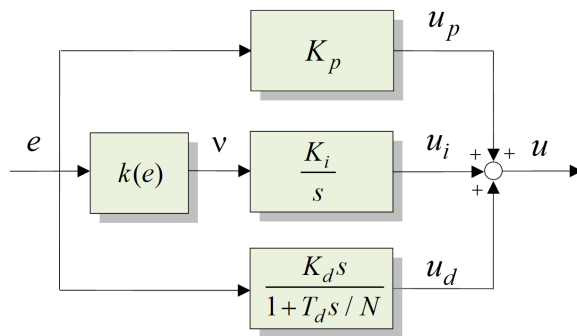


Figure 5. Structure of the NPID controller

3.2 The Enhanced Nonlinear PID Controller

The integral action of the above NPID controller nonlinearly scales down the error signal. This minimises the offset for small errors and prevents the excessive increase of the accumulated error and overshoot for large errors. This study employs an integral function to refine the nonlinear function defined in equation (13):

$$k(e) = a \exp\left[-\frac{e^2(t)}{2\sigma^2}\right], \quad (14)$$

where a is a positive constant. This nonlinear gain slightly increases the error to reduce the offset by increasing the accumulated error when the error is small. Substituting equation (14) in equation (12) yields:

$$v(t) = ae(t) \exp\left[-\frac{e^2(t)}{2\sigma^2}\right] \quad (15)$$

The constant a is chosen such that $v(t)$ assumes the value of $e(t)$ when $e(t)$ equals σ . By applying this to equation (15), a can be expressed as:

$$a = \frac{1}{\exp\left[-\frac{1}{2}\right]} = 1.6487 \quad (16)$$

From equation (14):

$$k(e) = 1.6487 \exp\left[-\frac{e^2(t)}{2\sigma^2}\right] \quad (17)$$

In this paper, σ is utilised, with a value that represents one-third of the biggest setpoint value difference. Figure 6 shows $v(t)$ obtained using $k(e)$ from equations (13) and (17) together with a typical value of $\sigma = 1$.

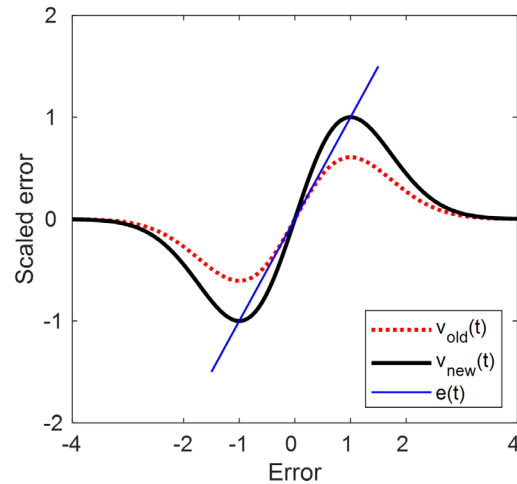


Figure 6. Scaled error plots of the two nonlinear functions

As it can be seen in Figure 6, the integral action of the conventional PID controller uses $e(t)$ as it is, but the enhanced $k(e)$ reaches a value greater than that of $e(t)$ while $e(t) < \sigma$, then it decreases rapidly and converges to 0 if $e(t)$ becomes bigger.

3.3 Tuning of the NPID controller

The tuning of the NPID controller covered in the previous subsection revealed the optimal parameters $\mathbf{P} = [K_p, K_i, K_d]^T \in \mathcal{S}$, where $\mathcal{S} = \{\mathbf{P} | \mathbf{P}^{(L)} \leq \mathbf{P} \leq \mathbf{P}^{(U)}\}$ is the search space, and $\mathbf{P}^{(L)}$ and $\mathbf{P}^{(U)}$ are the lower and upper bounds, respectively.

3.3.1 Performance Metrics

Adjusting a controller's settings impacts both its responsiveness to the desired setpoint and its ability to manage disturbances. These two settings are often in conflict. However, since the disturbances are commonly unmeasurable and unpredictable, the controller is tuned so as to have a good tracking performance. Optimising this problem requires defining a performance metric and using an algorithm to find the setting that minimises it. In the tuning of controller parameters, three commonly employed performance measures are the integral of absolute error (IAE), the integral of time-weighted absolute error (ITAE), and the integral of squared error (ISE) (Haji Haji & Monje, 2019). These measures are fundamentally based on error evaluation. In this study, to avoid a high control effort, two performance measures are used, namely the integral absolute error with control signal (IAEU) and integral time-weighted absolute error with control signal (ITAEU) defined as follows:

$$IAEU = \int_0^{t_f} \sum_{k=1}^2 (w_k |e_k(t)| + |\Delta u_k(t)|) dt, \quad (18a)$$

$$ITAEU = \int_0^{t_f} \sum_{k=1}^2 t (w_k |e_k(t)| + |\Delta u_k(t)|) dt, \quad (18b)$$

where $e_k(t)$ represents the error signal, defined as the difference between the output $y_k(t)$ and its corresponding setpoint, $\Delta u_k(t) = u_k(t) - u_{k0}$ is the deviation of the control input where u_{k0} is the steady-state value of $u_k(t)$ in equation (10), w_k is a weighting factor ($k=1,2$), and t_f is a sufficiently long simulation time. By adjusting the weighting factor, one can fine-tune how much each component contributes to the overall performance score.

3.3.2 Genetic Algorithms

To solve the optimisation problem, a genetic algorithm (GA) is utilised. The GA incorporates three key operations: selection, crossover, and mutation (Isayed & Hawwa, 2007) minimizing the overshoot and improving the required control effort during the functions of the read/write (R/W). The pseudocode for the GA is presented below:

Algorithm.
Set $t = 0$;
Create an initial population of individuals of length L ;
Evaluate the function value $f_i(t)$ of each individual;
while (termination is not met) do the following steps:
Set $t = t + 1$;
Apply selection;
Apply the crossover and mutation;
Evaluate the function value $f_i(t)$ of each individual;
end while

4. Simulation and Discussion

4.1 Gain Tuning for the NPID and PID Controllers

Step changes for the setpoint in the top composition y_{s1} from 83 to 93 and the bottom composition y_{s2} from 5 to 7 were introduced to take place at time 0 (min). The MATLAB GA function was employed to systematically search for the gain values that minimise IAEU or ITEAU. The weighting factors w_1 and w_2 in equations 18(a-b) were set at 0.2. The search bounds for the two controller gains for the top composition were constrained to the interval $[0, 1]$, while the search bounds for the bottom composition were set to $[-0.5, 1]$. The outcomes of this tuning process are included in Table 1 and Table 2.

Table 1. Tuned controller gains using IAEU

Controller	Top composition			Bottom composition		
	K_p	K_i	K_d	K_p	K_i	K_d
NPID	0.339	0.019	0.124	-0.130	-0.024	-0.137
PID	0.317	0.027	0.064	-0.129	-0.016	-0.085

Table 2. Tuned controller gains using ITAEU

Controller	Top composition			Bottom composition		
	K_p	K_i	K_d	K_p	K_i	K_d
NPID	0.374	0.123	0.418	-0.147	-0.039	-0.228
PID	0.354	0.178	0.418	-0.139	-0.052	-0.216

4.2 Controller Performance Assessment

This subsection evaluates the performance of the two controllers using time-domain metrics, focusing on setpoint tracking and disturbance rejection. For setpoint tracking, the overshoot (M_p), settling time (t_s), and integral of absolute error (IAE) are assessed. IAE is defined as follows:

$$IAE = \int_0^{t_f} |e_k(t)| dt, \tag{19}$$

where $e_k(t) = y_{sk} - y_k$ ($k=1,2$). For disturbance rejection, the perturbation peak (M_{peak}), recovery time (t_{rcy}), and IAE are evaluated. M_{peak} denotes the maximum deviation from the setpoint during a disturbance, while t_{rcy} represents the time required to return within 5% of the setpoint after a disturbance occurs.

4.2.1 Tracking Performance

A series of simulations were conducted to evaluate the effectiveness of the proposed NPID controller which was tuned by using a GA. Figures 7 and 8 show the tracking responses for the top and bottom compositions and the control input responses, respectively, for the two methods, each of them tuned for minimizing the IAEU from equation (18a). Meanwhile, Figures 9 and 10 depict the disturbance rejection responses and the control input responses for the same methods, each of them optimized for minimizing the ITAEU from equation (18b). Table 3 and Table 4 show the values of the performance indices for both approaches for both the top and bottom compositions. As it can be seen in Table 3, which shows the performance of the two controllers tuned based on the IAEU performance index, the M_p of the NPID controller has a slightly greater value in comparison with that obtained by the PID controller for the top composition whereas the values of the other two performance measures are lower than those obtained by the PID controller. Table 4, which shows the performance of the two controllers tuned based on the ITAEU, reveals that the NPID controller obtained lower values for almost all the performance metrics for both the top and bottom compositions. The overshoot M_p for the bottom composition is 60.38% for the PID controller. The settling time t_s for the top composition is 17.12 (min) for the NPID controller and 16.07 (min) for the PID controller, while for the bottom composition the t_s is 20.64

(min) for the NPID controller and 23.83 (min) for the PID controller.

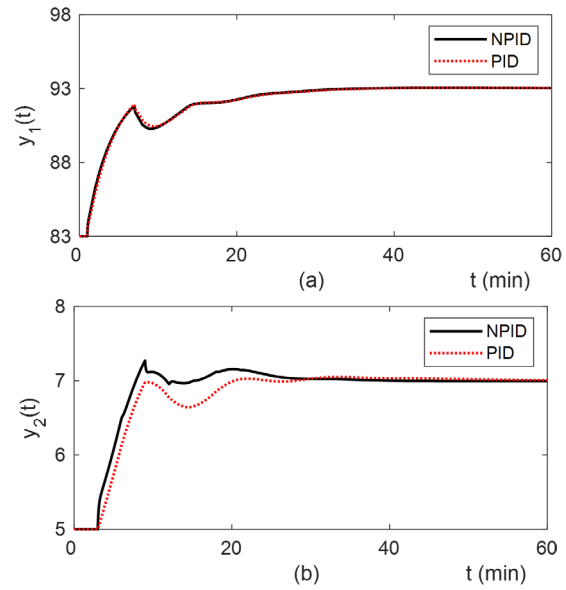


Figure 7. Tracking responses: (a) Top composition; (b) Bottom composition

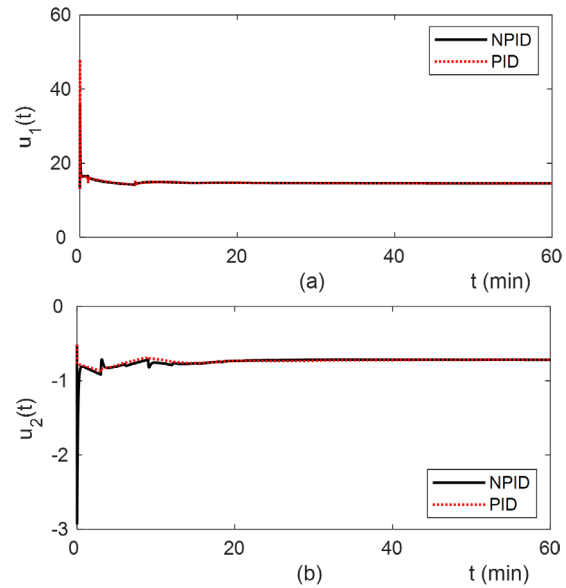


Figure 8. Control inputs: (a) Reflux flow rate; (b) Steam flow rate

Table 3. Setpoint tracking performance for IAEU

Controller	Top composition			Bottom composition		
	M_p	t_s	IAE	M_p	t_s	IAE
NPID	0.51	28.09	60.21	13.57	26.85	11.84
PID	0.44	28.81	60.69	2.58	36.98	14.79

Table 4. Setpoint tracking performance for ITAEU

Controller	Top composition			Bottom composition		
	M_p	t_s	IAE	M_p	t_s	IAE
NPID	30.00	17.12	30.58	36.98	20.64	11.13
PID	35.73	16.07	32.63	60.38	23.83	17.29

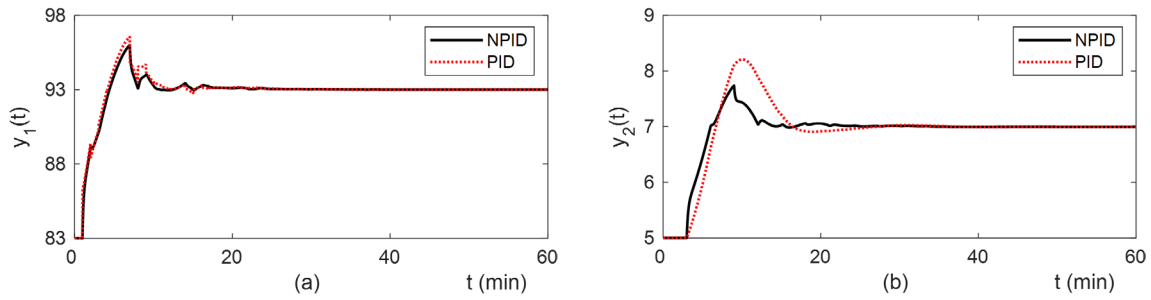


Figure 9. Tracking responses: (a) Top product composition; (b) Bottom product composition

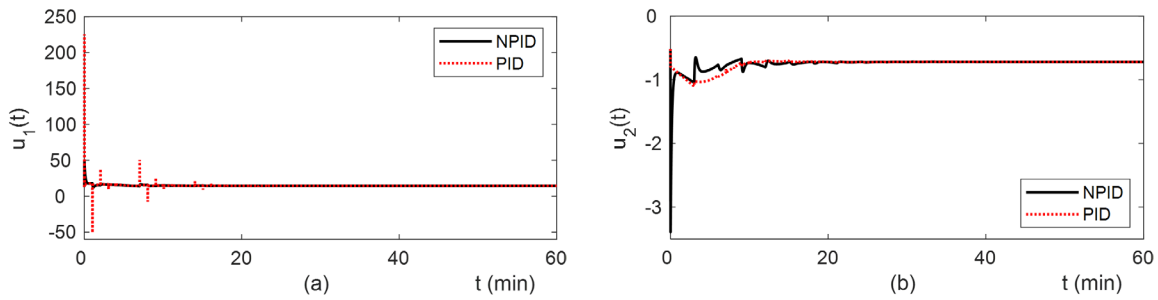


Figure 10. Control inputs: (a) Reflux flow rate; (b) Steam flow rate

4.2.2 Disturbance Rejection

To verify the disturbance rejection performance of the proposed method, a simulation was conducted in which a step change of the input feed rate of magnitude $d = 0.4$ was applied at 0 (min), while the outputs remained steady at the nominal state of $y_1(t) = 93$ and $y_2(t) = 7$. Figure 11 shows the disturbance rejection responses of the two methods tuned based on IAEU for the top and

bottom compositions, and Figure 12 shows the control input responses.

As it can be seen in Figures 11 and 12, the proposed controller recovers from the disturbance faster than the PID controller. A quantitative comparison of the two methods tuned based on both IAEU and ITAEU was conducted by calculating the M_{peak} , t_{rcy} , and IAE, the results of which are included in Table 5 and Table 6.

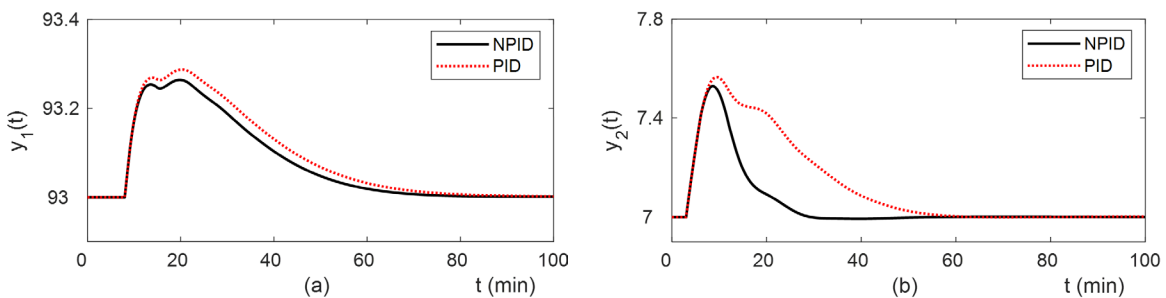


Figure 11. Disturbance rejection responses: (a) Top product composition; (b) Bottom product composition

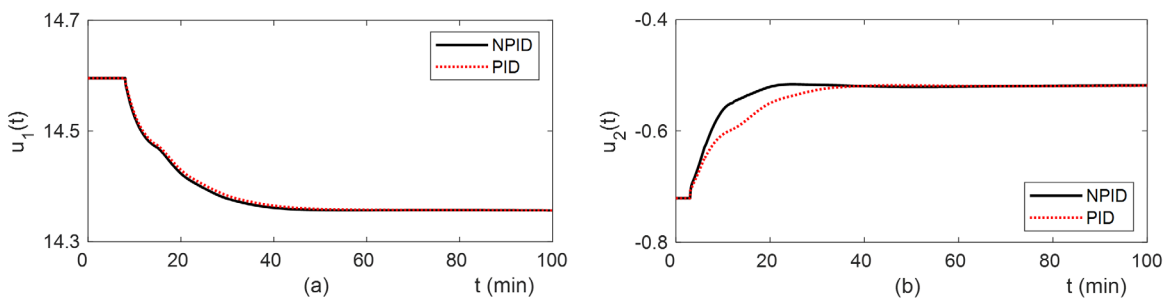


Figure 12. Control inputs: (a) Reflux flow rate; (b) Steam flow rate

Table 5. Disturbance rejection performance using IAEU

Controller	Top composition			Bottom composition		
	M_{peak}	t_{rcy}	IAE	M_{peak}	t_{rcy}	IAE
NPID	0.26	63.65	7.61	0.53	25.61	5.51
PID	0.29	69.71	8.95	0.56	49.07	12.64

Table 6. Disturbance rejection performance using ITAEU

Controller	Top composition			Bottom composition		
	M_{peak}	t_{rcy}	IAE	M_{peak}	t_{rcy}	IAE
NPID	0.17	26.75	1.19	0.48	27.28	3.86
PID	0.18	28.25	1.36	0.48	18.01	3.99

5. Conclusion

This study presents an NPID-based control method for a two-input, two-output DC process. The primary challenge in controlling a DC lies in the strong interactions between inputs and outputs. The appropriate decoupling techniques were applied to address this problem, effectively transforming the MIMO process into two independent single-input, single-output systems. Two enhanced NPID controllers were subsequently designed to control the distillate top and bottom compositions independently. A GA optimised the controller parameters by minimising the IAEU and ITAEU performance indices. In order to compare the proposed controller with the PID controller quantitatively, setpoint tracking

and disturbance rejection were evaluated using performance indices like M_p , t_s , M_{peak} , t_{rcy} , and IAE. The simulation results demonstrated that the proposed method featured a superior performance in comparison with the alternative method for controlling both the top and bottom compositions of the DC.

Anyhow, further research is required to apply the proposed control method in a real process and assess its effectiveness.

Acknowledgements

This research was supported by Korea Institute of Marine Science & Technology Promotion (KIMST) funded by the Ministry of Oceans and Fisheries (RS-2021-KS211489).

REFERENCES

- Acharya, P., Dumpa, G. & Dan, T. K. (2016) Modelling and control of distillation column. In: *2016 International Conference on Computation of Power, Energy Information and Communication (ICCPEIC), 20-21 April 2016, Melmaruvathur, India*. New York, USA, IEEE. pp. 123-128.
- Bhattacharjee, S. & Medhi, B. (2012) Soft Computing Techniques for Distillation Column Composition Control. In: Mathew, J., Patra, P., Pradhan, D. K. & Kuttyamma, A. J. (eds.) *Eco-friendly Computing and Communication Systems. ICECCS 2012 (Proceedings of the International Conference ICECCS 2012, 9-11 August 2012, Kochi, India, part of the book series Communications in Computer and Information Science*, vol. 305). Berlin, Heidelberg, Germany, Springer, pp. 381-388.
- Carrasco, B., Ávila, E., Vitoria, A. et al. (2021) Shrinking-Core Model Integrating to the Fluid-Dynamic Analysis of Fixed-Bed Adsorption Towers for H₂S Removal from Natural Gas, *Energies*. 14(17), art. no. 5576. <https://doi.org/10.3390/en14175576>.
- Das, D., Chakraborty, S. & Naskar, A. K. (2023) Controller design on a new 2DOF PID structure for different processes having integrating nature for both the step and ramp type of signals. *International Journal of Systems Science*. 54(7), 1423-1450. <https://doi.org/10.1080/00207721.2023.2177903>.
- Fard, A. N., Shahbazian, M., & Hadian, M. (2016). Adaptive Fuzzy Controller Based on Cuckoo Optimization Algorithm for a Distillation Column. In: *2016 International Conference on Computational Intelligence and Applications (ICCIA), 27-29 August 2016, Jeju, Korea (South)*. New York, USA, IEEE. pp. 93-97.
- Govinda, K. E. & Arunshankar, J. (2022) Control of TITO processes using sliding mode controller tuned by ITAE minimizing criterion based Nelder-Mead algorithm. *Chemical Product and Process Modeling*. 17(6), 669-680. <https://doi.org/10.1515/cppm-2020-0120>.
- Haji Haji, V. & Monje, C. A. (2019) Fractional-Order PID Control of a MIMO Distillation Column Process Using Improved Bat Algorithm. *Soft Computing*. 23(18), 8887-8906. <https://doi.org/10.1007/s00500-018-3488-z>.
- Hamdy, M. & Ramadan, A. (2017) Design of Smith Predictor and Fuzzy Decoupling for MIMO Chemical Processes with Time Delays. *Asian Journal of Control*. 19(1), 57-66. <https://doi.org/10.1002/asjc.1338>.
- Isayed, B. M. & Hawwa, M. A. (2007) A Nonlinear PID Control Scheme for Hard Disk Drive Servosystems. In: *2007 Mediterranean Conference on Control & Automation, 27-29 June 2007, Athens, Greece*.

- New York, USA, IEEE. <https://doi.org/10.1109/MED.2007.4433790>.
- Jin, G.-G. & Son, Y.-D. (2019) Design of a Nonlinear PID Controller and Tuning Rules for First-Order Plus Time Delay Models. *Studies in Informatics and Control*. 28(2), 157-166. <https://doi.org/10.24846/v28i2y201904>.
- Li, J., Li, S., Li, S. et al. (2015) Neural-network-based composite disturbance rejection control for a distillation column. *Transactions of the Institute of Measurement and Control*. 37(9), 1146-1158. <https://doi.org/10.1177/0142331214558681>.
- Nevetha, P. B. & Suresh, M. (2016) Design of Decoupler and Performance Analysis of Distillation Column. *International Journal of Innovative Research in Electrical, Electronics, Instrumentation and Control Engineering*, 4(6), 40–43. <https://doi.org/10.17148/IJIREEICE.2016.4610>.
- Nourelhouda, F. & Abdelmadjid, K. (2022) Fractional PID controller based on biggest log modulus tuning method with MOPSO optimization for distillation column. *Indonesian Journal of Electrical Engineering and Computer Science*. 28(3), 1396-1404. <https://doi.org/10.11591/ijeecs.v28.i3>.
- O'Dwyer, A. (2009) *Handbook of PI and PID Controller Tuning Rules*. 3rd ed. London, Imperial College Press.
- Pawar, R. N. & Jadhav, S. P. (2018) Design of NDT and PSO based decentralised PID controller for Wood-Berry distillation column. In: *2017 IEEE International Conference on Power, Control, Signals and Instrumentation Engineering (ICPCSI), 21-22 September 2017, Chennai, India*. New York, USA, IEEE pp. 719-723.
- Son, Y.-D. & Jin, G. G. (2019) A Nonlinear PD Controller Design and its Application to MOV Actuators. *Studies in Informatics and Control*. 28(1), 5-12. <https://doi.org/10.24846/v28i1y201901>.
- Tan, H. & Cong, L. (2023) Modeling and Control Design for Distillation Columns Based on the Equilibrium Theory. *Processes*. 11(2), art. no. 607. <https://doi.org/10.3390/pr11020607>.
- Wood, R. K. & Berry, M. W. (1973) Terminal composition control of a binary distillation column. *Chemical Engineering Science*. 28(9), 1707-1717. [https://doi.org/10.1016/0009-2509\(73\)80025-9](https://doi.org/10.1016/0009-2509(73)80025-9).
- Ye, L., Zhang, N., Li, G. et al. (2023) Intelligent Optimization Design of Distillation Columns Using Surrogate Models Based on GA-BP. *Processes*. 11(8), art. no. 2386. <https://doi.org/10.3390/pr11082386>.



This is an open access article distributed under the terms and conditions of the Creative Commons Attribution-NonCommercial 4.0 International License.